

Article

Mineralization Process of MVT Zn-Pb Deposit Promoted by the Adsorbed Hydrocarbon: A Case Study from Mayuan Deposit on the North Margin of Sichuan Basin

Guiyuan Guan ¹, Siwen Li ^{2,*} and Rongxi Li ^{1,3,*}¹ School of Earth Science and Resources, Chang'an University, Xi'an 710051, China² Key Laboratory of Subsurface Hydrology and Ecology in Arid Areas, Department of Environmental Engineering, School of Water and Environment, Chang'an University, Xi'an 710051, China³ Key Laboratory of West Mineral Resources and Geological Engineering of Ministry of Education, Chang'an University, Xi'an, 710051, China

* Correspondence: swli@chd.edu.cn (S.L.); rongxli@chd.edu.cn (R.L.); Tel.: +86-151-2901-3624 (S.L.); +86-137-0926-6389 (R.L.)

Abstract: The Mayuan Zn-Pb deposit on the northern margin of the Sichuan Basin is rich in Zn-Pb deposit resources. Additionally, a large amount of bitumen is observed in outcrops, and these deposits represent a key template for exploring the migration of hydrocarbon fluids and metal elements within an ancient oil reservoir. In this study, a chemical experimental method was used to extract the adsorbed hydrocarbon from the chosen five groups of samples, and mathematical statistical methods were also used. The varied metal concentrations before and after the extraction experiments have been noticed, due to the direct carrying action of the adsorbed hydrocarbon. In addition, a strong correlation was observed between the Mayuan Zn-Pb deposit and their source rocks, as well as the same distribution trend from the rare earth element distribution curve. A moderate correlation was observed between the two groups of black shales and Mayuan Zn-Pb ores, and the rare earth partition curve showed consistent trends. The results show that organic matter exists in two forms, among which hydrocarbon organic matter is extracted due to the carrying effect of extraction experiment, and the remaining non-hydrocarbon organic matter is combined with metal elements to form a metal complex. Hydrocarbons are involved in mineralization, asphaltenes are derived from bitumen, and one of the potential sources of Pb/Zn in the Mississippi Valley type (MVT) Zn-Pb deposit is black shale rich in organic matter.

Keywords: Mayuan zinc-lead deposit; adsorbed hydrocarbon; chemical experiment; rare earth distribution; black shales



Citation: Guan, G.; Li, S.; Li, R. Mineralization Process of MVT Zn-Pb Deposit Promoted by the Adsorbed Hydrocarbon: A Case Study from Mayuan Deposit on the North Margin of Sichuan Basin. *Minerals* **2023**, *13*, 72. <https://doi.org/10.3390/min13010072>

Academic Editor: Maria Boni

Received: 28 November 2022

Revised: 28 December 2022

Accepted: 29 December 2022

Published: 1 January 2023



Copyright: © 2023 by the authors. Licensee MDPI, Basel, Switzerland. This article is an open access article distributed under the terms and conditions of the Creative Commons Attribution (CC BY) license (<https://creativecommons.org/licenses/by/4.0/>).

1. Introduction

Various types of Zn-Pb deposits are observed worldwide, including the two major types, Mississippi Valley-type (MVT) deposits and Sedimentary-Exhalative (SedEx) deposits. The MVT Zn-Pb deposit is the second largest Pb-Zn deposit type in the world, and its reserves and total amount account for 24% and 23% of all types of Zn-Pb deposits worldwide [1], respectively. A large number of studies have shown that MVT Pb-Zn deposits are closely related not only to oil and gas fields in terms of spatial distribution but also to hydrocarbon fluids in terms of their genesis. Many MVT Zn-Pb deposits exist in the world, such as the MVT Zn-Pb deposit [2], Nanisivik Zn-Pb ore deposit [3], Irish and Scottish Pb and Zn mines [4], and Nunavut Polaris Zn-Pb mine in Canada [5]. The symbiosis of Zn-Pb ore deposits and bitumen in space implies the close genetic relationship between Zn-Pb ore deposits and oil and gas. Reports have indicated that mining operations have used oil and gas deposits to find metal deposits. For example, bitumen was used as a prospecting guide to identify a MVT Zn-Pb deposit in western Canada [6]. The abnormal concentration of

natural gas in Irish Zn-Pb deposits also provided an important clue in the search for new Zn-Pb deposits [7].

Studies have also found that the formation of Zn-Pb deposits is closely related to hydrocarbon fluids. For example, Gu et al. (2010) showed that crude oil and its derivatives directly provide reducing sulfur or act as reducing agents in sulfate reduction reactions for MVT Zn-Pb mineralization [8]. Gao et al. (2016) suggested that an organic reducing fluid rich in CH₄ and H₂S was the key factor for the mineralization of the Mayuan large Zn-Pb deposit in the northern margin of Sichuan Basin, China. They further indicated that the ancient oil and gas reservoirs under high temperature thermochemistry were transformed into high-sulfur gas reservoirs; this provided a reducing organic fluid that was mixed with basin brine rich in Zn-Pb ions and then reacted to achieve mineralization [9].

Numerous studies have found that most of the world's large MVT Zn-Pb deposits and oil and gas fields coexist in foreland basin uplift or dome roof zones, which is consistent with the trend of oil and gas accumulation. Moreover, Zn-Pb deposits occur in a carbonate breccia-shaped (mainly dolomite) layer [10], where dissolution and pore development take place because of the high porosity and permeability, and such layers represent good reservoir space and traps, thus resulting in ideal hydrocarbon accumulation conditions [10]. Ore-forming fluid is characterized by high-salinity brine and enrichment in H₂S, HS⁻, and S²⁻ [10,11]. Additionally, the metallogenic temperature is nearly consistent with the oil and gas formation temperature (60–250 °C) [12]. Moreover, hydrocarbon fluids, solid asphalt, and oil or gas inclusions are observed in these layers, and the ore-forming fluids are characterized by abnormally high pressure. Zn-Pb ore deposit mineralization and oil and gas accumulation are related to regional convergent tectonic events, which are consistent with the time of formation of foreland structures [13–15].

The close relationship between MVT Zn-Pb deposits and hydrocarbon fluids has been widely recognized. Based on the direct or indirect involvement of hydrocarbon fluids in mineralization, multiple metallogenic models of MVT Zn-Pb deposits have been established, such as the following three models established by Sverjensky et al. (1986) [10]: (1) excess sulfur mineralization model, in which Pb and Zn migrate with oil field brine, which undergoes precipitate mineralization after encountering and mixing with sulfate-rich fluid; (2) sulfate reduction model, in which Pb and Zn migrate in sulfate-containing fluid or oil field brine, sulfate reduces to sulfide after encountering reductants, such as oil, gas, organic matter, or methane, and then precipitate mineralization occurs; and (3) reduced sulfur model, in which Pb, Zn, and reduced sulfur migrate in the same fluid and precipitate for mineralization due to changes in pH and temperature. In 2015, Anderson et al. (2015) [16] indicated that hydrocarbon fluids in oil and gas fields play three different roles in Pb and Zn mineralization: activator, carrier, and reducing agent. In addition, Saintilan et al. (2019) suggested that Pb, Zn, and other metal elements in the MVT Zn-Pb ore deposit migrate in two forms: organic (organometallic complex) and inorganic (compound), among which the organo-Pb/Zn complex is the most important migration form and accounts for 40–60% of the MVT Zn-Pb ore deposit [17].

However, controversy remains, and further discussion is required on the migration mode of Pb and Zn elements in the form of either compounds or organic Zn-Pb metal complexes in hydrocarbon fluid and the phase within which the minerals are being transported (liquid hydrocarbon or adsorbed hydrocarbon). If hydrocarbon fluids stably migrate with Pb and Zn, then the adsorbed hydrocarbons in ores and bitumen should contain high amounts of Pb/Zn. Therefore, this study investigated whether Pb and Zn migrated along with adsorbed hydrocarbons based on experimental analyses of the Pb and Zn contents in bitumen and ore from the large Mayuan MVT Zn-Pb mine in the Dabashan foreland basin.

2. Geological Setting

The study area is located in the Daba Mountain foreland Basin, the northern margin of the Yangtze block in the Sichuan Basin, and the southern side of the Hannan ancient continent in the south Qinling orogenic belt, namely the DFB area marked in the figure

(Figure 1). The core of the Biba core complex dome structure is composed of metamorphic rocks of the Huodiya Group of the Middle and Late Proterozoic and the intrusive complex of the Jining-Chengjiang period, while the outward sedimentary cover from the core of the dome is distributed in ring form from the Sinian Dengying Formation (Z_2dn) to the Early Middle Triassic (T_{1+2}) (Figure 1). A parallel unconformity contact relationship (ϵ_1/Z_2dn) is observed between the carbonaceous shale of the Dengying Formation and the Guojiaba Formation of the Lower Cambrian (equivalent to the Niuditang Formation in the Yangtze Region), and sedimentary discontinuities are observed between the Cambrian and Ordovician and the Silurian and Permian, which indicates that frequent tectonic activity occurred in this area during the sedimentary period [18].

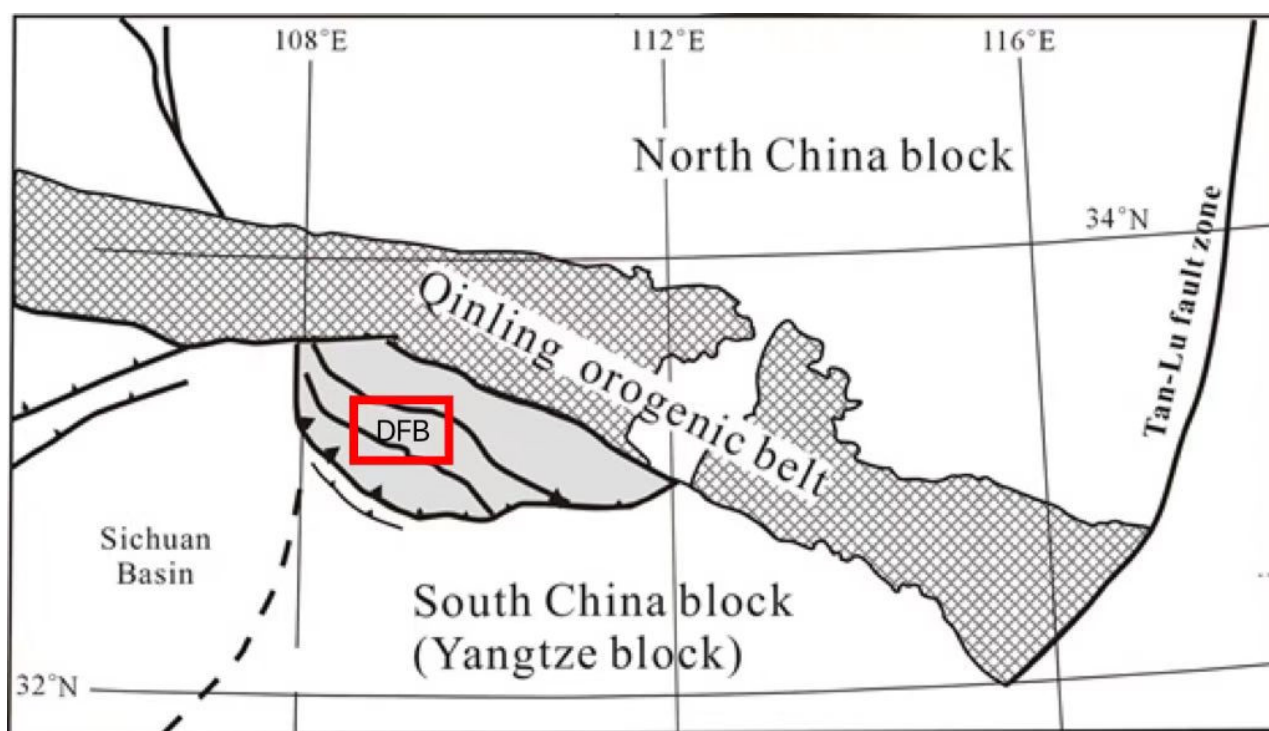


Figure 1. Geotectonic location map of the study area.

The Mayuan Zn-Pb deposit occurs in the breccia dolomite of the Dengying Formation (Z_2dn), which is divided into upper and lower members according to lithology. The lower member of the Dengying Formation (Z_2dn_1) consists of a set of clastic rock series composed of conglomerate and quartz sandstone with a complex composition, and it is directly unintegrated onto the basement complex at a high angle. The upper member of the Dengying Formation (Z_2dn_2) consists of a set of carbonate rocks that can be divided into four lithologic layers from bottom to top. The first lithologic section ($Z_2dn_2^1$) consists of stratified gray-white fine crystal dolomite; the second section ($Z_2dn_2^2$) consists of a siliceous band of dolomite; the third section ($Z_2dn_2^3$) consists of brecciated dolomite, which is an important natural gas layer on the Yangtze platform that frequently hosts MVT Zn-Pb deposits [11–14]; and the fourth member ($Z_2dn_3^4$) consists of laminated dolomite containing a diazote layer overlain by carbonaceous shale of the Lower Cambrian Guojiaba Formation [19] (Figure 2).

Zn-Pb mineralization mainly occurs in breccia dolomite, which is produced in bedding under the control of the interlayer fracture zone. Sphalerite is the main ore mineral, followed by galena. Gangue minerals mainly include dolomite and calcite. Previous studies have shown that the ore-forming temperature is primarily between 150 and 250 °C, and the salinity of the ore-forming fluid is mainly 8–25% NaCl, which is typical of a MVT Zn-Pb deposit [20–22]. Zn/Pb and other metals are derived from the black shale of the Guojiaba

Formation of the Lower Cambrian and the black shale of the Longmaxi Formation of the Lower Silurian, which consist of subbasement crystallized rocks. A large number of CH₄ and H₂S rich fluid inclusions have been found in sphalerite, dolomite, and other minerals, and their composition and isotope contents are consistent with the characteristics of natural gas in the Puguang gas field [23,24]. A large amount of solid bitumen and ore minerals co-exist in brecciated dolomite pores. Comparative analyses of the biomarkers show that the source rocks of bitumen and natural gas inclusions are consistent with those of the Puguang gas field, namely, the black shale of the Guojiaba Formation of the Lower Cambrian and the black shale of the Longmaxi Formation of the Lower Silurian.

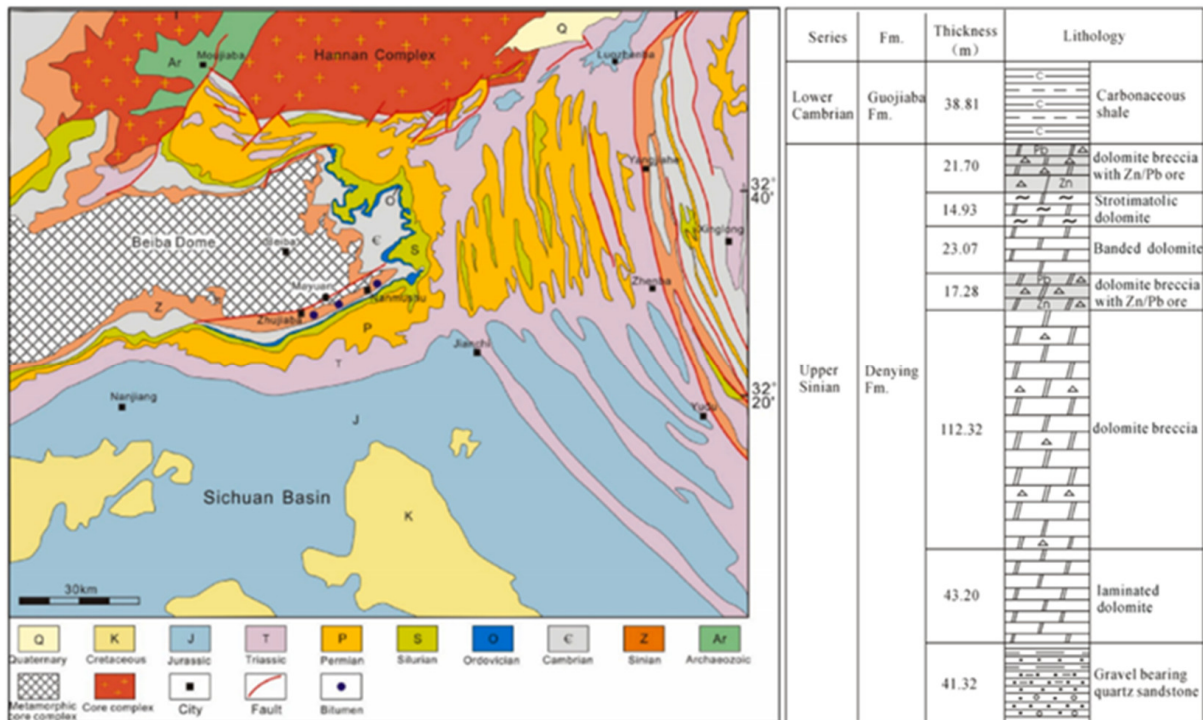


Figure 2. Simple geology map of the Beiba Dome on the northern margin of Sichuan basin, as well as sampling locations in Mayuan.

3. Materials and Methods

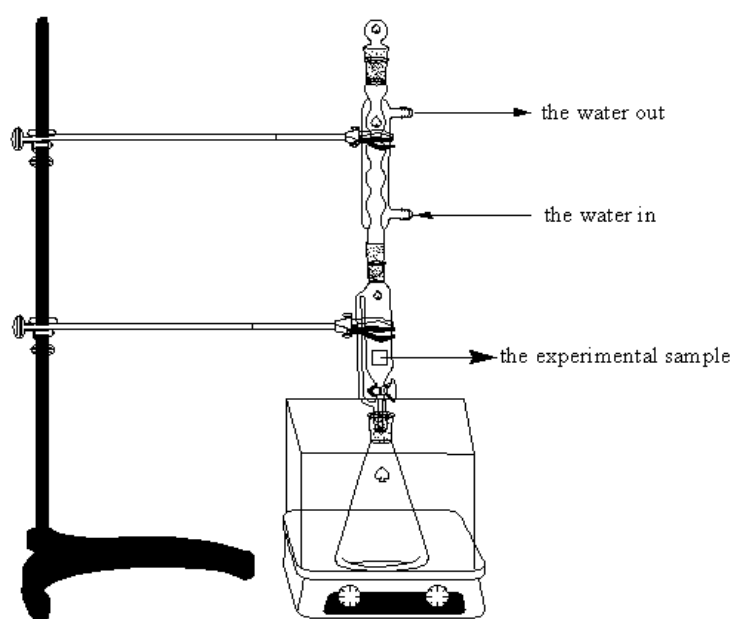
Samples of asphaltene sphalerite, solid bitumen, and asphaltene dolomite in the Mayuan Zn-Pb deposit were selected for the experiment, and the potential source beds of the Mayuan Zn-Pb deposit, namely the black shale samples of the Lower Cambrian Guojiaba Formation and the Lower Silurian Longmaxi Formation, were collected at the same time (Table 1). The sample grinding size was 200 mesh, and a certain amount of samples were sent to the Key Laboratory of Western Mineral Resources and Geological Engineering of Ministry of Education, Chang’an University for trace element analysis and testing by inductively coupled plasma analysis (ICP). After that, 10 g of each sample was selected, and the extraction experiment was carried out with chloroform (CHCl₃, 1.492 g/mL) using a Soxhlet extraction instrument, which could show the excellent extraction effect of organic matter.

The experimental process was to wrap 10 g of the weighed sample with degreased filter paper, put it into a 250 mL suction tube, add 200 mL CHCl₃ solution to the reaction flask, and extract the sample several times at 70 °C (Figure 3). After 72 h, the sample was recovered and analyzed by ICP-MS.

Table 1. Sample number table in the study area.

Sample Number	Sampling Point	Horizon	Sample Name
A	Fucheng township	Dengying Formation ore-bearing bed	Bitumen
B	Fucheng township	Dengying Formation ore-bearing bed	Asphaltene dolomite
C	Mayuan Zn-Pb mining area	Dengying Formation ore-bearing bed	Asphaltene sphalerite
D	Fucheng township	Guojiaba Formation	Black shale
E	Fucheng township	Longmaxi Formation	Black shale
A ₁	Fucheng township	Dengying Formation ore-bearing bed	Bitumen ^a
B ₁	Fucheng township	Dengying Formation ore-bearing bed	Asphaltene dolomite ^a
C ₁	Mayuan Zn-Pb mining area	Dengying Formation ore-bearing bed	Asphaltene sphalerite ^a
D ₁	Fucheng township	Guojiaba Formation	Black shale ^a
E ₁	Fucheng township	Longmaxi Formation	Black shale ^a

^a is the solid recovery product after the extraction experiment.

**Figure 3.** Chemical diagram of the extraction experiment.

4. Results

Table 2 shows that the contents of trace elements in five samples analyzed by ICP differed before and after the extraction experiment. The following parameters were reported for the extraction experiment and test: (1) Changes of certain trace elements and extraction rates of the five groups of samples after extraction; (2) Pearson correlation coefficients and distribution patterns of rare earth elements in bitumen, dolomite, and sphalerite of the Mayuan Zn-Pb deposit; and (3) Pearson correlation coefficients and distribution patterns of rare earth elements in the two groups of black shale and the Mayuan Zn-Pb deposit (asphalt, dolomite, and sphalerite). A multivariate statistical analysis method based on cluster analysis was performed in this study to assess the changes in trace elements and extraction rates after continued extraction. IBS SPSS Statistics 22 software was used for the analyses. Pearson correlation coefficients and a rare earth partition model were used in the correlation analyses between the Mayuan Zn-Pb ore deposit and black shale.

Table 2. The content of trace elements in the Mayuan Zn-Pb deposit (ppm).

Elements	A	A ₁	B	B ₁	C	C ₁	D	D ₁	E	E ₁
Li	0.90	0.82	0.70	0.65	1.42	1.36	16.10	15.91	25.87	25.55
Be	0.03	0.03	0.03	0.03	0.05	0.05	1.69	1.67	2.24	2.20
Sc	0.84	1.36	1.24	1.58	1.64	1.94	14.32	14.01	10.14	9.97
V	10.2	8.46	7.80	10.23	12.08	12.77	328.4	326.8	238.9	229.8
Cr	8.26	7.90	3.53	4.68	3.83	4.19	86.21	86.12	53.14	52.28
Co	1.30	1.31	1.92	1.89	2.15	2.22	4.95	5.01	13.04	12.89
Ni	8.73	8.44	11.19	10.56	10.26	10.41	70.81	71.60	92.28	90.86
Cu	2.19	2.25	113.8	110.9	178.0	183.7	12.73	12.58	56.33	55.63
Zn	951.9	882.5	36,727	32,665	61,201	53,940	177.1	145.2	519.6	426.1
Ga	0.17	0.15	3.53	3.47	5.14	5.29	17.62	17.83	14.25	13.96
Rb	0.58	0.65	0.45	0.48	1.98	2.03	80.86	72.06	103.54	102.95
Sr	28.01	27.86	40.62	39.89	55.05	55.67	75.59	73.39	70.53	70.52
Y	0.43	0.44	0.89	0.81	1.06	1.05	28.66	28.58	22.48	23.15
Zr	0.52	0.36	0.32	0.33	1.58	1.59	295.4	279.7	141.8	141.2
Nb	0.07	0.08	0.05	0.05	0.16	0.17	12.41	12.67	16.92	16.91
Mo	0.48	0.48	1.39	1.81	1.97	1.90	16.97	17.25	19.43	19.70
Cd	3.36	3.45	505.9	500.9	781.2	771.8	1.58	1.49	4.70	4.16
In	0.00	0.00	0.12	0.11	0.22	0.22	0.04	0.04	0.06	0.07
Cs	0.03	0.02	0.07	0.06	0.25	0.24	3.78	3.88	6.30	6.22
Ba	21.14	20.32	15.72	14.09	36.26	36.32	926.2	923.1	900.5	894.5
La	0.33	0.28	0.45	0.39	0.69	0.75	32.48	32.37	33.71	33.38
Ce	0.62	0.57	1.04	0.93	1.53	1.66	64.92	63.94	63.11	62.83
Pr	0.09	0.08	0.17	0.15	0.22	0.23	7.81	7.80	7.62	7.54
Nd	0.37	0.33	0.76	0.67	0.88	1.02	29.42	29.60	28.38	28.28
Sm	0.07	0.07	0.16	0.16	0.21	0.21	5.49	5.48	5.60	5.47
Eu	0.03	0.03	0.05	0.05	0.06	0.06	1.34	1.35	1.23	1.28
Gd	0.10	0.09	0.16	0.18	0.23	0.21	5.60	5.76	5.72	5.60
Tb	0.01	0.01	0.02	0.02	0.03	0.03	0.84	0.83	0.77	0.77
Dy	0.07	0.04	0.15	0.12	0.17	0.16	4.97	4.96	4.02	4.15
Ho	0.01	0.01	0.03	0.02	0.04	0.03	1.05	1.05	0.80	0.82
Er	0.03	0.03	0.07	0.06	0.10	0.10	3.28	3.26	2.42	2.40
Tm	0.00	0.00	0.01	0.01	0.01	0.01	0.47	0.48	0.33	0.33
Yb	0.03	0.02	0.04	0.04	0.09	0.06	3.15	3.16	2.24	2.19
Lu	0.00	0.00	0.01	0.01	0.01	0.01	0.48	0.50	0.33	0.34
Hf	0.01	0.01	0.01	0.01	0.04	0.05	8.20	8.69	3.98	3.96
Ta	0.02	0.01	0.03	0.02	0.03	0.02	0.97	0.98	1.20	1.18
Pb	7.56	7.31	1213	1161	1215	1150	17.99	15.81	28.21	26.15
Bi	0.01	0.00	0.01	0.02	0.05	0.04	0.26	0.28	0.45	0.45
Th	0.05	0.04	0.06	0.04	0.18	0.17	12.23	13.36	11.16	11.30
U	0.56	0.56	0.74	0.75	0.60	0.61	21.79	22.33	12.44	12.63
Li	0.90	0.82	0.70	0.65	1.42	1.36	16.10	15.91	25.87	25.55

4.1. Comparison Results of Samples before and after the Extraction Experiment

The changes before and after the extraction experiment were compared and discussed by combining the ICP data of the samples with the element clustering pedigree map. Samples A, B, C, A₁, B₁, and C₁ had excessive Zn contents. High proportions among all trace elements were determined via the element content data, which are shown in Table 2. For the samples from the ore-bearing bed, the Zn content of three kinds of rock elements was too high and showed values two orders of magnitude higher than that of the other elements. This was because of the inability of the singular element content to cluster with other trace elements that presented differences in content, which affected the clustering of other metal elements found at low levels. Therefore, the Zn element was removed from the clustering pedigree diagram of six samples of ore-bearing strata in the Dengying Formation after extraction, and only the clustering pedigree diagram of the remaining 39 elements was displayed.

Figure 4a shows the element clustering pedigree diagram of sample A, where 39 trace elements are clustered. As shown in the figure, the element clustering of the bitumen samples containing mineral layers from the Dengying Formation are divided into three categories, with Sr and Ba grouped into one category; Cr, Ni, Pb, and V grouped into another category; and the remaining 33 elements (including Mo) grouped into the final category. First, 33 elements, including Cr, Ni, Pb, V, and Mo, were clustered, and then Sr and Ba were clustered. Figure 4 shows the element clustering pedigree diagram of sample A₁, namely sample A, after conducting the siphon experiment.

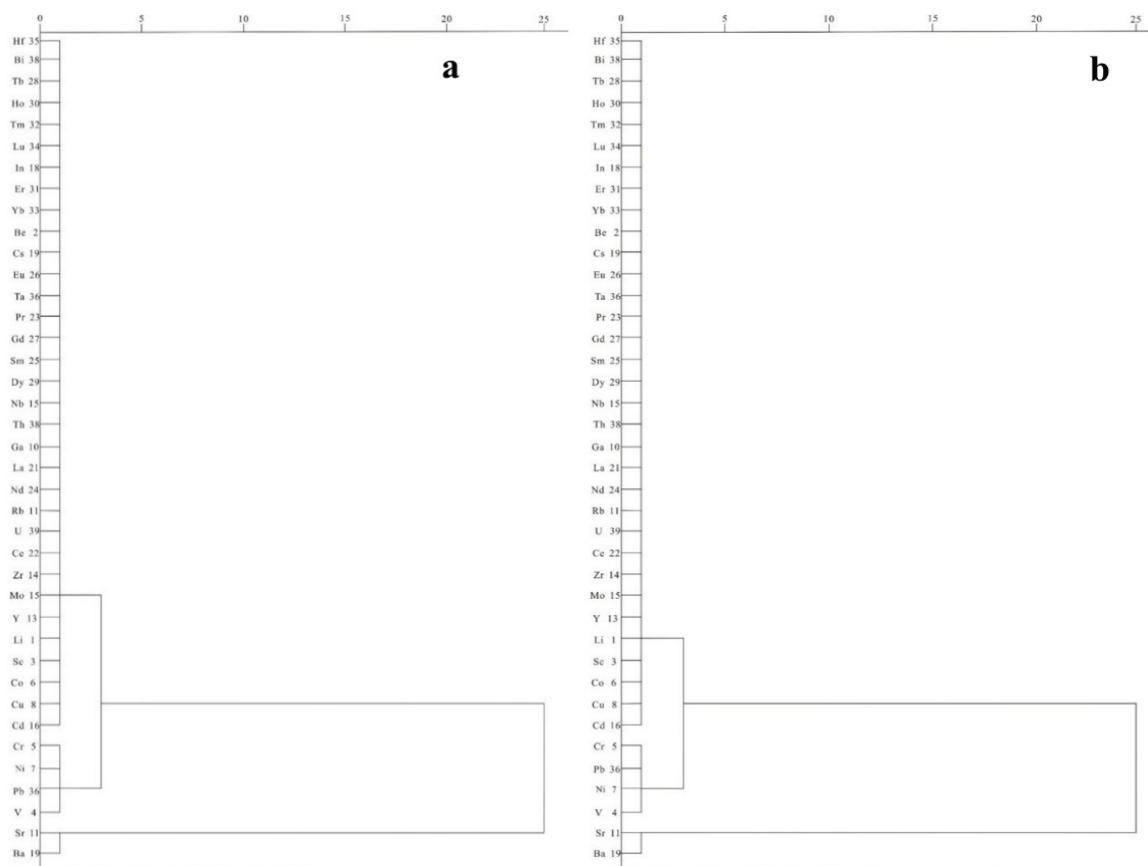


Figure 4. Pedigree diagram of element clustering in samples A (a) and A₁ (b).

Table 3 shows that the content of Zn in sample A₁ was the highest at 882.5 ppm, while the contents of Sr and Ba reached 27.86 and 20.32 ppm, respectively, and Cr, Pb, Ni, and V reached 7.90, 7.31, 8.44, and 8.46 ppm, respectively. When the elemental content of Sr and Ba was three or four times that of Cr, Pb, Ni, and V, as shown in Table 4, we can deduce that Sr and Ba belonged to the same category while Cr, Pb, Ni, and V belonged to the same category. By comparing the element clustering spectrum of the bitumen of the Dengying Formation before the extraction experiment with sample A (Figure 4a), we found that the classification was consistent.

Table 3. Comparison the element content changes in samples A and A₁ (ppm).

Elements	Zn	Pb	Cd
B	36,727	1213	505.9
B ₁	32,666	1161	500.9
ΔB ^a	11.1%	4.3%	1.0%

$$\Delta B^a = (B - B_1) / B \times 100\%.$$

Table 4. Comparison element content changes in samples B and B₁ (ppm).

Elements	Zn	Sr	Ba	Cr	Pb	Ni	V
A	951.9	28.01	21.14	8.26	7.56	8.73	10.2
A ₁	882.5	27.86	20.32	7.90	7.31	8.44	8.46
ΔA ^a	7.49%	0.53%	3.87%	4.36%	3.31%	3.32%	1.75%

$$\Delta A^a = (A - A_1) / A \times 100\%.$$

Figure 5a shows the element clustering pedigree diagram of the class B sample. The clustering results of the 39 elements in this sample could be divided into three categories: Pb and Cd were grouped into their own category, and the remaining 37 elements, including Ba, were classified into another category. First, 37 elements, including Ba and Cd, were clustered with Pb. As shown in Figure 5b, sample B₁ reflects the element clustering pedigree of sample B after the siphon experiment, and it was divided into three categories: Cd was grouped into one category, Pb was grouped into another category, and the other 37 elements were grouped into the final category. As shown in Table 4, the content of Zn in sample B₁ reached 32,666 ppm. The content of Zn was the highest among all trace elements, which was similar to sample B, followed by Cd and Pb at 500.9 and 1161 ppm, respectively. In Figure 5b, Zn is not shown due to its high content. Among the 39 trace elements, Cd was clustered with the other 37 elements first and then with Pb. A comparison of the cluster pedigree map with the dolomite in the Dengying Formation before the extraction experiment shows that the classification was consistent before and after extraction. The extraction rates of Zn and Pb before and after the experiment were 11.1% and 4.3%, respectively.

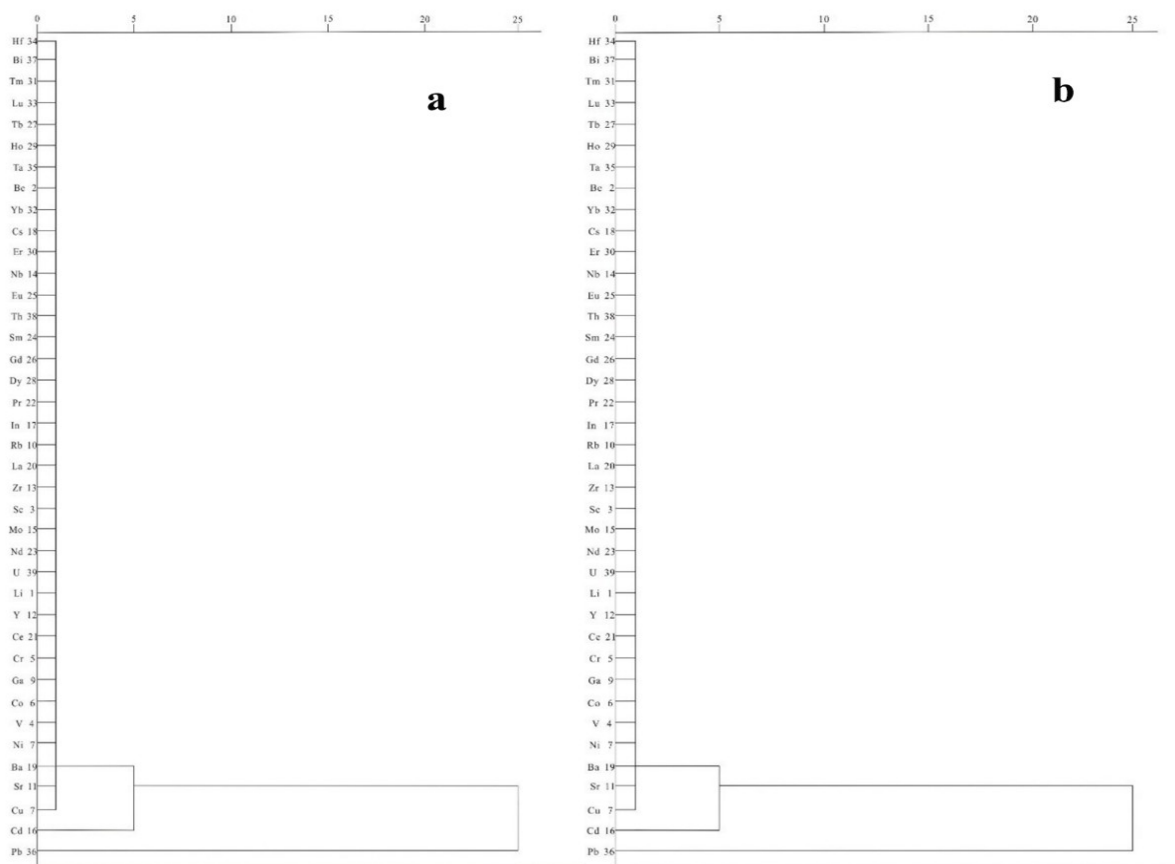


Figure 5. Pedigree diagram of element clustering in samples B (a) and B₁ (b).

Figure 6a shows the element clustering pedigree diagram of sample C. The clustering results of 39 elements in this sample are shown in the figure, which can be divided into two categories: Cd and Pb were grouped into one category, and 37 elements, including Ni,

were grouped into another category. These two groups were clustered together into a final category. As shown in Figure 6b, the element clustering pedigree diagram of sample C₁ (sample C after the extraction experiment) was divided into two categories: Cd and Pb were clustered into one category, and the other 37 elements were grouped into another category. As shown in Table 5, the content of Zn in sample C₁ reached 53,940.12 ppm, which was consistent with that in sample C, and the content of Zn was the highest among all trace elements, followed by Cd and Pb at 771.85 and 1150 ppm, respectively. In Figure 6b, Zn was not shown in the figure due to its high content. The clustering of the other 39 trace elements showed that Cd and Pb clustered together first, followed by the other 37 elements. A comparison with the clustering pedigree diagram of sample C in Figure 6a did not reveal significant differences in classification. The differences in the main trace elements between the two samples after the extraction are shown in Table 5. The contents of Zn, Pb, and Cd were 11.9%, 5.33%, and 1.27%, respectively.

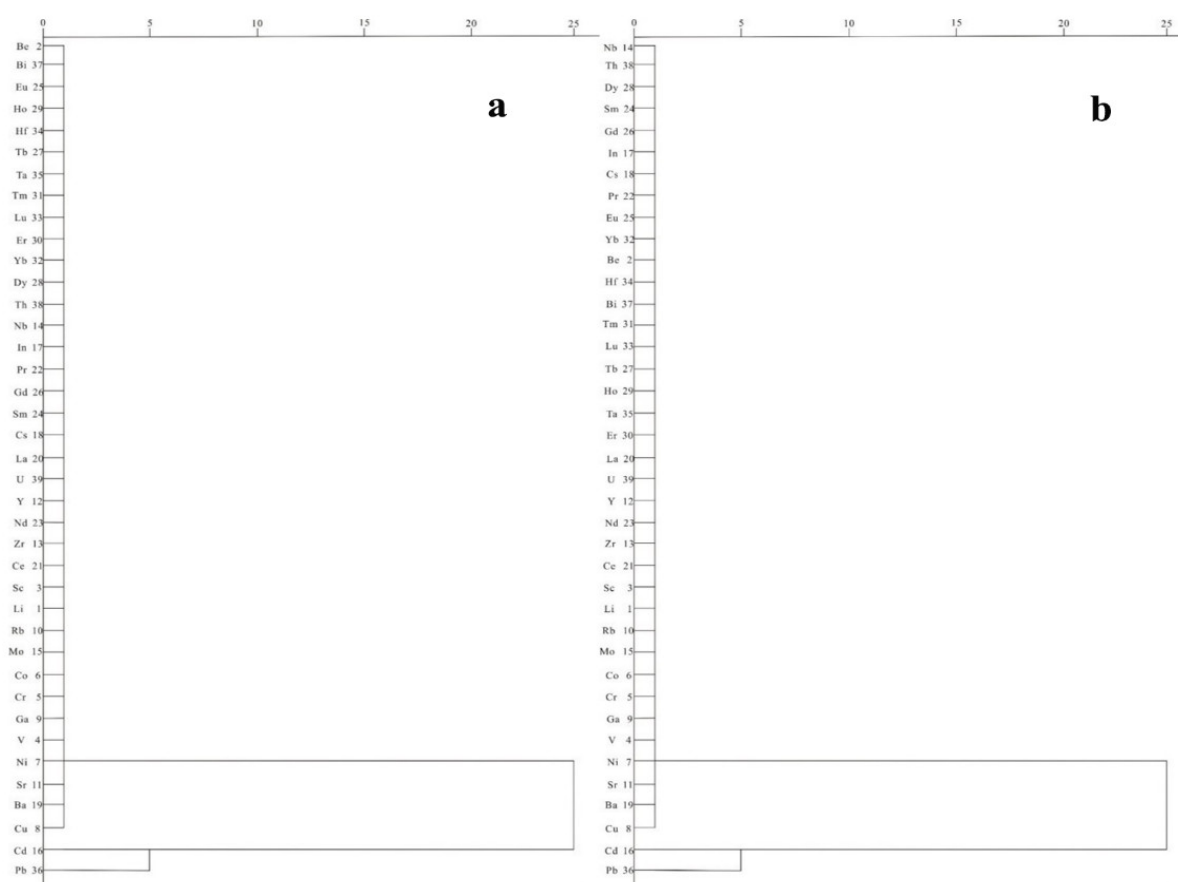


Figure 6. Pedigree diagram of element clustering in samples C (a) and C₁ (b).

Table 5. Comparison element content changes in samples C and C₁ (ppm).

Elements	Zn	Pb	Cd
C	61,201	1215	781.2
C ₁	53,940	1150	771.8
ΔC ^a	11.9%	5.33%	1.27%

$$\Delta C^a = (C - C_1) / C \times 100\%.$$

Figure 7a shows the element clustering pedigree diagram of sample D. The results of the 40 elements clustering in the sample are shown in the figure, and they can be divided into three categories: 36 elements (including U) were grouped into one category; V, Zr, and Zn were grouped into another category and Ba was grouped by itself into a final category.

During the grouping, 36 elements (including U, V, Zr, and Zn) were clustered first and then grouped with Ba. As shown in Figure 7b, sample I included the element clustering pedigree of sample D after the siphon experiment. In the figure, 40 elements were divided into three categories: V and Zr were classified into one category, Ba was classified into another category, and the other 37 elements were classified into a final category. In Table 6, changes are observed in the main elements in the black shale before and after the experiment. As shown in Table 6, before and after the extraction experiment, the content of Zn changed the most, reaching 18%, while the content of V, Zr, and Ba changed 0.47%, 5.32%, and 0.33%, which was far less than that of Zn. Table 7 shows that the contents of V, Zr, and Ba in sample I were 326.8, 279.7, and 923.1 ppm, respectively. Additionally, as shown in Figure 7a, elements V and Zr were grouped together, and 37 trace elements (excluding V, Zr, and Ba) were clustered and finally grouped with Ba. A comparison with the clustering pedigree diagram of sample D in Figure 7 shows that the elements in the black shale of the Guojiaba Formation are roughly consistent before and after the extraction experiment. For example, the Ba elements are grouped separately, while the V and Zr elements are clustered together. However, the major difference between the groups was the clustering of Zn. Before the extraction experiments, Zn, V, and Zr were classified as a class, whereas after the experiment, Zn did not cluster with the other two elements. In addition to V, Zr, and Ba, 36 kinds of trace elements were included in the rest of the cluster, which corresponded to the Guojiaba.

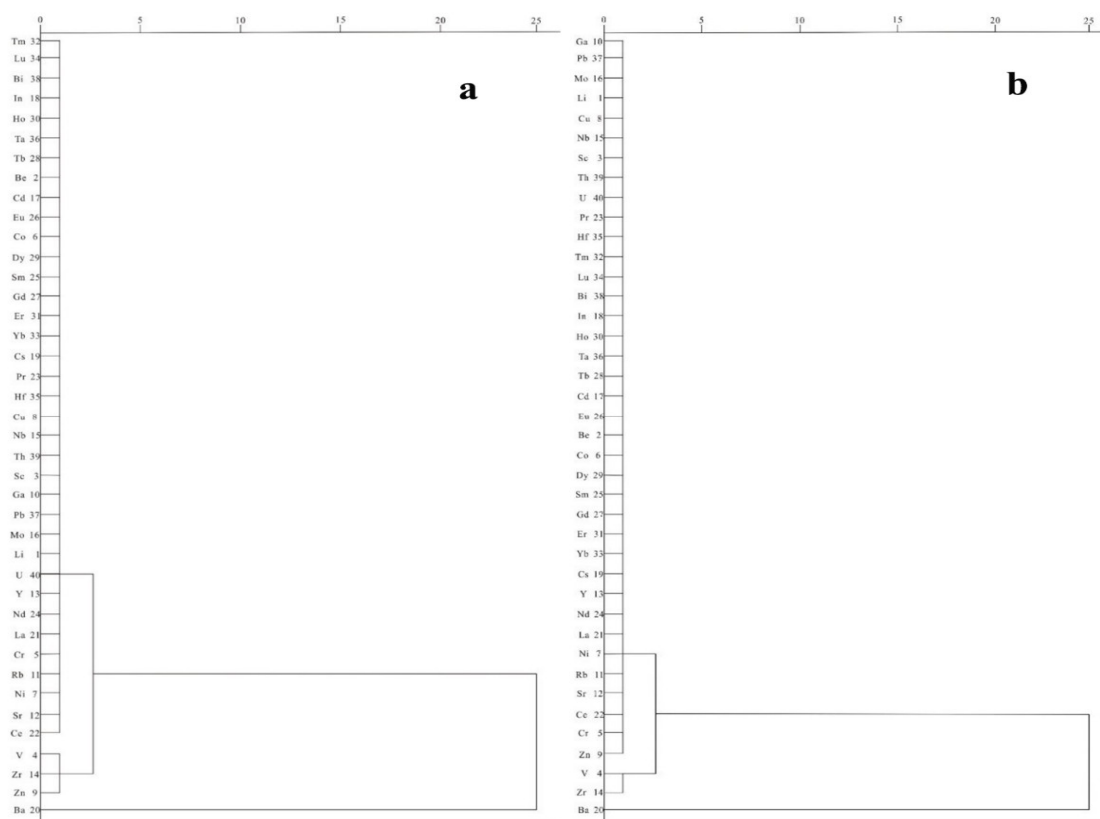


Figure 7. Pedigree diagram of element clustering in samples D (a) and D₁ (b).

Table 6. Comparison element content changes in samples D and D₁ (ppm).

Elements	Zn	V	Zr	Ba
D	177.1	328.4	295.4	926.2
D ₁	145.2	326.8	279.7	923.1
ΔD	18.0%	0.47%	5.32%	0.33%

$$\Delta D = (D - D_1) / D \times 100\%$$

Table 7. Comparison table of content changes in samples E and E₁ (ppm).

Element Type	Zn	V	Zr	Ba
E	519.6	238.9	141.8	900.5
E ₁	426.1	229.8	141.2	894.5
ΔE	18.0%	3.80%	0.45%	0.67%

$$\Delta E = (E - E_1) / E \times 100\%$$

Figure 8a shows the element clustering pedigree diagram of sample E. The results of the clustering of 40 elements are shown in the figure, and they can be divided into three categories: 36 elements (including Nd) were grouped into one category; V and Zr were grouped into another category; and Ba and Zn were grouped into a final category. First, 36 elements (including Nd) were clustered with V and Zr and then with Ba and Zn. As shown in Figure 8b, the element clustering pedigree diagram of sample E₁ (sample E after the siphon experiment) shows that 40 trace elements can be divided into three categories: V and Zr clustered into one category, Zn and Ba elements clustered into another category, and the remaining 36 trace elements clustered into a final category. Table 7 shows that the contents of V, Zr, Zn, and Ba in sample E₁ were 229.8, 141.2, 426.1, and 894.50 ppm, respectively. Additionally, Figure 8b shows that V and Zr first clustered into a group together, then with the remaining 36 trace elements, then with Zn, and finally with Ba. Changes in the element content of the black shale of the Longmaxi Formation before and after the extraction experiment are shown in Table 7. Zn was the most well-transported trace element, reaching 18.0% of the initial content. The main elements in samples E and E₁ were V, Zr, and Ba, and they were transported in amounts of 3.80, 0.45, and 0.67%, respectively.

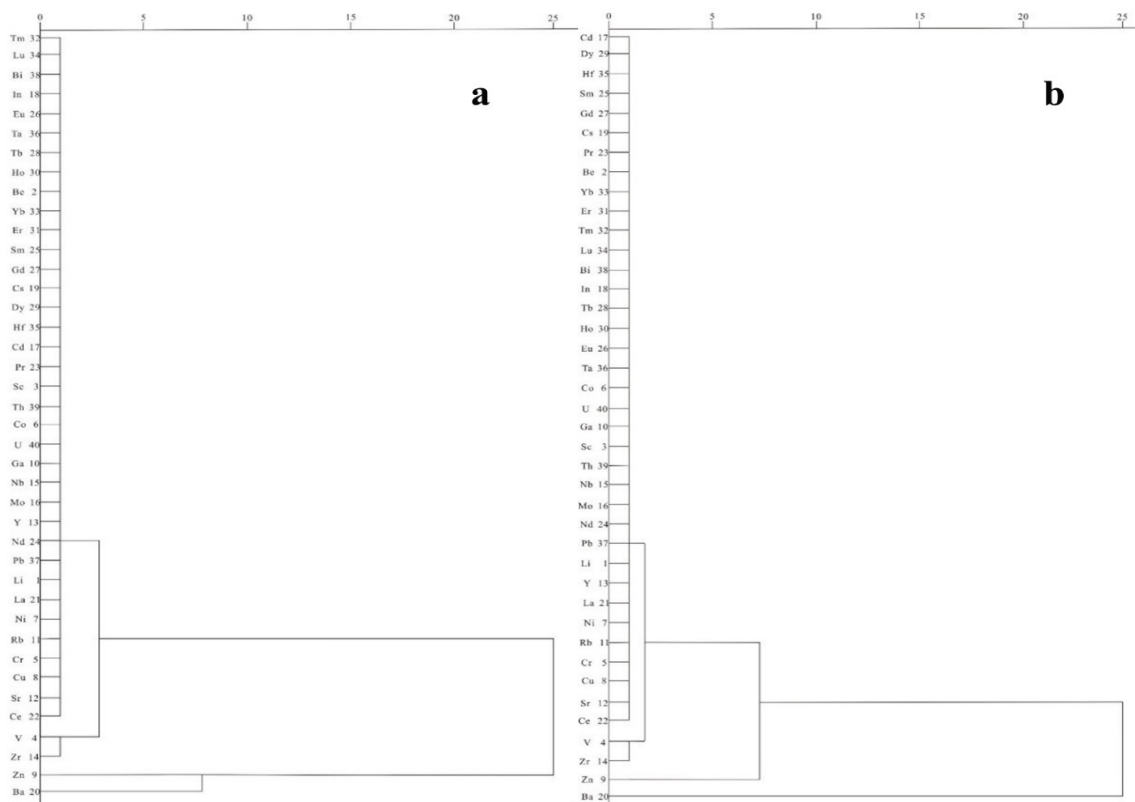


Figure 8. Pedigree diagram of element clustering in samples E (a) and E₁ (b).

4.2. Pearson Correlation Coefficient and Rare Earth Partition Model of the Mayuan Zn-Pb Deposit

The focal research elements of the Mayuan Zn-Pb deposit in samples A, B, and C are bitumen, dolomite, and sphalerite from the Dengying Formation, respectively. The Pearson

correlation coefficients of the three groups of samples were calculated and discussed using 40 trace elements as indicators, and then the rare earth elements of the three groups of samples were standardized based on comparisons with spheroidal meteorites.

As shown in Table 8, the Pearson correlation coefficients were used to explore the correlations among the three ores in the same Mayuan area. The correlation coefficients between samples A and B and between A and C were 0.999, while that between sample B and C was 1.000. The significance among the three comparisons was 0.00.

Table 8. Correlation test table of Mayuan Zn-Pb deposit (pearson correlation significance).

Sample Number	A	B	C
Sample A	1	0.999	0.999
	0.000	0.000	0.000
Sample B	40	40	40
	0.999	1	1.000
Sample C	0.000	0.000	0.000
	40	40	40

Table 9 shows the contents of the 14 rare earth elements in the three ores and the corresponding values in spheroidal meteorites. The total amounts of rare earth elements (Σ REE) in the three ores were 1.76, 3.14, and 4.61 ppm, among which the total amount of light rare earth (Σ LREE) ranged from 1.51 to 3.93 ppm and the total amount of heavy rare earth (Σ HREE) ranged from 0.25 to 1.18 ppm. The rare earth partition curves after standardization are shown in Figure 9.

Table 9. Analysis results of rare earth elements in the Mayuan Zn-Pb deposit (ppm).

Sample Number	A	B	C	Chondrite Values
La	0.33	0.45	0.75	0.31
Ce	0.62	1.04	1.66	0.81
Pr	0.09	0.17	0.23	0.12
Nd	0.37	0.76	1.02	0.6
Sm	0.07	0.16	0.21	0.2
Eu	0.03	0.05	0.06	0.07
Gd	0.1	0.18	0.23	0.26
Tb	0.01	0.02	0.03	0.05
Dy	0.07	0.15	0.17	0.32
Ho	0.01	0.03	0.04	0.07
Er	0.03	0.07	0.10	0.21
Tm	0	0.01	0.01	0.03
Yb	0.03	0.04	0.09	0.21
Lu	0	0.01	0.01	0.03
Σ LREE	1.51	2.63	3.93	2.11
Σ HREE	0.25	0.51	0.68	1.18
Σ REE	1.76	3.14	4.61	3.29

Note: Chondrite data are quoted from W.V.Boynton [25], Σ LREE = La + Ce + Pr + Nd + Sm + Eu, Σ HREE = Gd + Tb + Dy + Ho + Er + Tm + Yb + Lu.

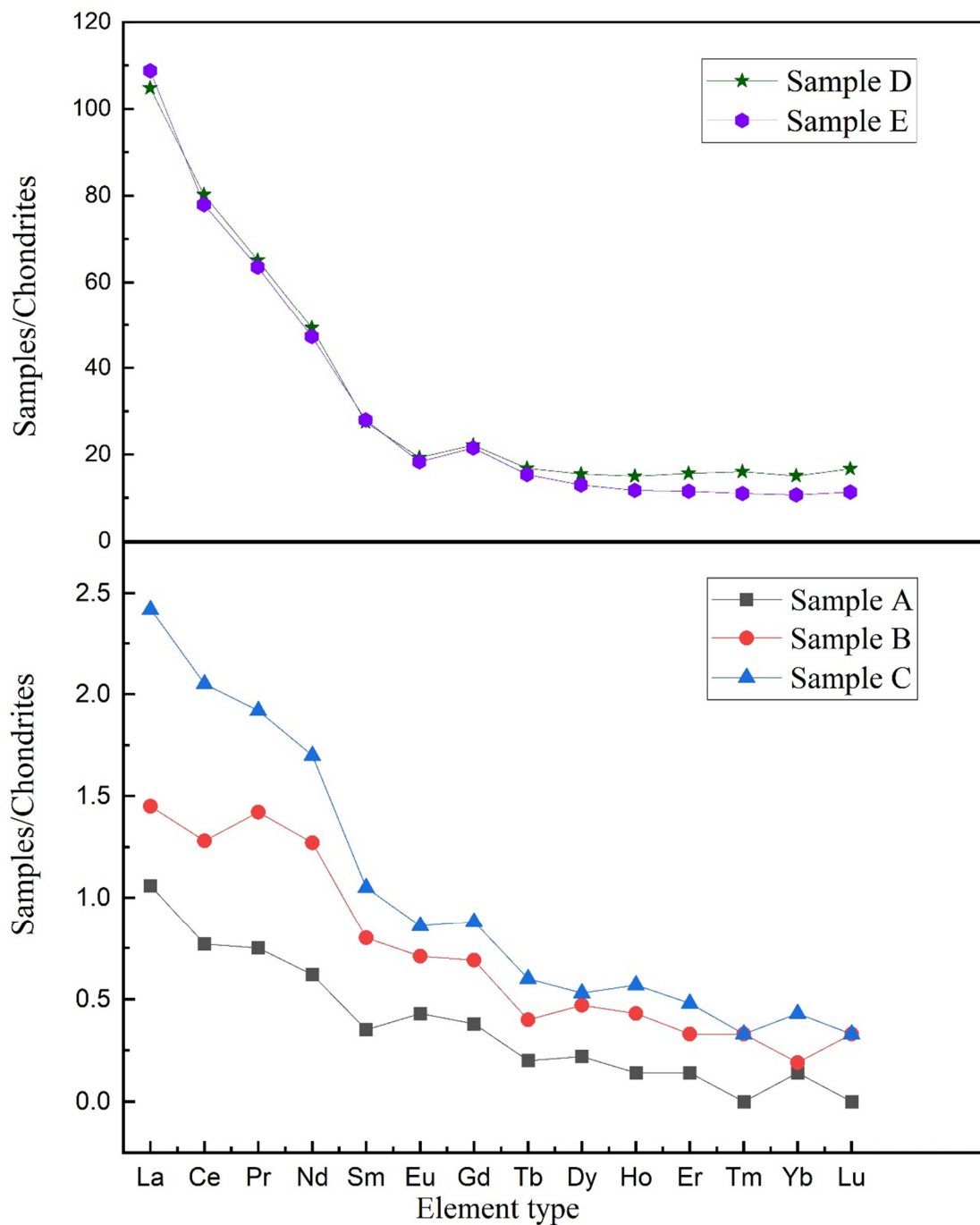


Figure 9. REE distribution patterns normalized to spheroid meteorites from the Mayuan Zn-Pb ore and black shale.

4.3. Correlation Analysis between Black Shale and Mayuan Zn-Pb Deposits

The focal research elements of black shale are included in samples D and E, which are sourced from the black shale of the Guojiaba Formation and the black shale of the Longmaxi Formation, respectively. The focal research elements of the Mayuan Zn-Pb deposit are shown in samples A and C, which include the bitumen and sphalerite of the Dengying Formation. Four samples were selected as the observation objects. The correlations between samples A and C of the Mayuan Zn-Pb deposit and samples D and E of two groups of black shale were assessed based on Pearson correlation coefficients, and the rare earth elements of the four groups of samples were standardized based on comparisons with spheroidal meteorites.

As shown in Table 10, Pearson correlation coefficients were used to explore the correlations between bitumen in sample A and sphalerite in sample C from the Mayuan Zn-Pb deposit area, black shale in sample D from the Guojiaba Formation, and black shale in sample E from the Longmaxi Formation. The correlation coefficients between samples A and D, A and E, and C and D were 0.142, 0.474, and 0.119, respectively. The correlation coefficient between samples C and E was 0.453, while that between the black shale samples D and E was 0.924. The contents of 14 rare earth elements and the corresponding spheroid meteorite values of the black shales of the Guojiaba Formation and the Longmaxi Formation are displayed in Table 11. The Σ REE of the two black shale samples were 161.69 and 156.37; the Σ LREE values were 141.65 and 139.7; and the Σ HREE values were 0.25 and 1.18. The distribution patterns of normalized REE elements in spheroid meteorites from the Mayuan Zn-Pb deposit and black shale samples are shown in Figure 9.

Table 10. Correlation test of the Mayuan Zn-Pb deposit (Pearson correlation significance).

Sample Number	A	C	D	E
Sample A	1	0.999	0.142	0.474
	40	0.000	0.381	0.002
Sample C	0.999	1	0.119	0.453
	0.000	40	0.464	0.003
Sample D	0.142	0.119	1	0.924
	0.381	0.464	40	0.000
Sample E	0.474	0.453	0.924	1
	0.002	0.003	0.000	40

Table 11. Analysis results of rare earth elements in black shale (ppm).

Sample Number	D	E	Chondrite Values
La	32.48	33.71	0.31
Ce	64.92	63.11	0.81
Pr	7.81	7.62	0.12
Nd	29.60	28.38	0.6
Sm	5.49	5.60	0.2
Eu	1.35	1.28	0.07
Gd	5.76	5.60	0.26
Tb	0.84	0.77	0.05
Dy	4.97	4.15	0.32
Ho	1.05	0.82	0.07
Er	3.28	2.42	0.21
Tm	0.48	0.33	0.03
Yb	3.16	2.24	0.21
Lu	0.50	0.34	0.03
Σ LREE	141.7	139.7	2.11
Σ HREE	20.04	16.67	1.18
Σ REE	161.7	156.4	3.29

Note: Chondrite data are quoted from W.V.Boynnton, Σ LREE = La + Ce + Pr + Nd + Sm + Eu, Σ HREE = Gd + Tb + Dy + Ho + Er + Tm + Yb + Lu.

5. Discussion

The analysis and discussion are mainly divided into the following three parts: (1) exploring the carrying capacity of hydrocarbon fluid for metal elements based on a comparison of the trace element content data after extraction; (2) performing a correlation analysis of the asphalt, dolomite, and sphalerite based on Pearson correlation coefficients and rare earth partition model diagrams; and (3) performing a correlation analysis between

the black shale and Mayuan Zn-Pb deposit (asphalt, dolomite, and sphalerite) based on Pearson correlation coefficients and rare earth partition model diagrams.

5.1. Conjecture on the Type of Organic Matter during the Mineralization

According to ICP data in Table 2, it can be seen that among the five samples, asphalt, asphaltene dolomite, and asphaltene sphalerite have the highest content of Zn. By observing the changes of the three samples of Mayuan Zn-Pb deposit before and after the extraction experiment, it can be found that Zn has a significant decrease trend before and after the extraction experiment; for example, the change rate of Zn in bitumen reaches 7.49%, and the mixed bitumen of Mayuan Zn-Pb deposit has Zn variation rates of asphaltic dolomite and asphaltic sphalerite are 11.1% and 11.9%, respectively. The asphaltic dolomite and asphaltic sphalerite formed by mixing bitumen with dolomite and sphalerite not only retain the original characteristics of the two ores, but also highlight the high content of some metal elements in bitumen, especially the content of Zn element. Therefore, the content of Zn element in three kinds of Mayuan Zn-Pb deposit in the collected samples is very high, far exceeding the 1.3 ppm required for MVT mineralization [26]. The comparison before and after the extraction test showed that the Zn element of the three was carried by chloroform effectively. The experimental data significantly indicated that hydrocarbon fluids can effectively carry some metal elements. The Zn element in the three Mayuan Zn-Pb deposits in this experiment is one of the metal elements with the best content in the source rocks and the most obvious extraction effect before and after the extraction experiment. ZnS is the main component of sphalerite. This also demonstrates that hydrocarbon fluids can effectively carry the mixed basin brine when flowing through the source rocks with sufficient Zn content and then react to mineralization.

By observing the cluster lineages of 39 trace elements of bitumen, dolomite, and sphalerite before and after the extraction experiment in Figures 4–6, it is found that the element cluster system before and after the extraction experiment has not changed significantly, and the main metal elements maintain a stable cluster structure. This may be because organic matter exists in the forms of hydrocarbon and non-hydrocarbon, in which hydrocarbon organic matter is effectively extracted with the Zn element and the remaining non-hydrocarbon organic matter is combined with the other metallic elements in the form of a complex. The remaining non-hydrocarbon organic matter and metallic elements do not have significant change characteristics and changes, so the cluster system remains unchanged after extraction. The stable cluster system before and after the extraction experiment also proved that the hydrocarbon fluid carried some metal elements, especially Zn elements, while the non-hydrocarbon form of organic matter formed complexes with the remaining metal elements and cooperated with various trace elements to construct a stable cluster system consistent with the extraction advance.

5.2. The Correlation Analysis of Asphaltene Samples and Their Metal Carrying Capacity

Pearson correlation coefficients and rare earth element partition curves were used to explore the correlation among the three kinds of Pb and Zn ores: bitumen, dolomite, and sphalerite. Among them, the Pearson correlation coefficient was 0.999 between bitumen and dolomite, 1.000 between dolomite and sphalerite, and 0.999 between bitumen and sphalerite ($p = 0.00$). From the Pearson correlation coefficient data, the correlation of the Mayuan Zn-Pb deposit is extremely strong.

During the extension of geological history, the elemental geochemical characteristics of different types of rocks are affected to some extent. Therefore, the influence of late geological processes should be excluded within a reasonable range when geochemical analysis is carried out. Rare earth elements have high chemical stability and are relatively difficult to change in sedimentary diagenesis [27]. Therefore, rare earth elements can be used as a reliable index to compare the similarity of three samples. The REE distribution curves of the three Mayuan Zn-Pb deposits are similar, showing the relative enrichment of light REE elements and the relative depletion of heavy REE elements. The variation

trends of Σ REE, Σ LREE, and Σ HREE of the three kinds of ores all show a right-leaning trend. The three ore samples were taken from the vicinity of the Mayuan Zn-Pb mining area, and the genesis and formation environments of bitumen, asphaltene dolomite, and asphaltene sphalerite are similar. The three samples, asphalt, asphaltene dolomite, and asphaltene sphalerite, all of which contain a certain amount of organic matter, show similar geochemical behavior before and after the extraction experiment and do not change the characteristics of the clustering system. Through the nearly perfect Pearson correlation coefficient of the three samples, combined with the clustering system of the three samples, it can be directly concluded that the three samples have similar elemental composition structures. The late metallogenic genesis and forming environment are consistent. Asphalt outcrops can be seen in the Mayuan Zn-Pb deposit in the field, and they are associated with sphalerite and dolomite. The results show that organic matter is the effective carrier of metal elements in the basin brine formed by hydrothermal reduction of Pb/Zn ores. Asphaltene was formed under the action of geological outcrop during oil and gas cracking and later stages. Therefore, combined with the strong correlation between the three samples, it can be inferred that the organic matter in asphaltene dolomite and asphaltene sphalerite is derived from asphalt, which is used to carry metal elements in the late mineralization process and then reaction mineralization.

5.3. Correlation Analysis between the Mayuan Zn-Pb Deposit and Black Shale

The correlation between the Mayuan Zn-Pb deposit (bitumen, asphaltene sphalerite) and black shale (black shale of the Guojiaba Formation and Longmaxi Formation) was explored by Pearson correlation coefficients and rare earth element partition curves. The correlations between the two groups of Mayuan Zn-Pb deposits and the two groups of black shale show that the bitumen of sample A and the sphalerite of sample C were moderately correlated with the black shale of sample E from the Longmaxi Formation and weakly correlated with the black shale of sample D from the Guojiaba Formation. Although the two groups of black shale are from different strata, their formation environment and development processes were likely similar, and they may be the sources of metal elements for the Mayuan Zn-Pb deposit. The Pearson correlation coefficient was 0.142 between the bitumen and black shale of the Guojiaba Formation, 0.119 between the sphalerite and black shale of the Guojiaba Formation, 0.474 between the bitumen and black shale of the Longmaxi Formation, and 0.453 between the sphalerite and black shale of the Longmaxi Formation. The two kinds of Mayuan Zn-Pb deposits showed strong correlations with the black shale of the Longmaxi Formation and a weak correlation with the black shale of the Guojiaba Formation. However, the Pearson correlation coefficient of the two groups of black shale was 0.924, thus showing a strong correlation.

Rare earth elements are not susceptible to weathering, thermal alteration, or metamorphism and have high chemical stability. Thus, rare earth elements are effective geochemical indicators for correlations among the provenance when excluding the influence of various natural processes in later geological evolution and geological history [27]. The rare earth distribution curves of four kinds of rocks were similar to those of samples A, C, D, and E, and they were also similar to those of the samples of light rare earth element concentrations. A relative deficit of relatively heavy rare earth elements was observed. Samples A and C from the Mayuan Zn-Pb deposit include bitumen and sphalerite from the Dengying Formation, and strong correlations were observed between these samples. Therefore, the source of sphalerite in samples A and C must be the same, and the organic matter and metal elements in both samples were likely contributed by the same lithology. On the rare earth partition curve, the two groups of black shale showed the same trend and presented right-leaning curves, and these shales showed strong correlations. Thus, the source and formation process of the two groups of black shale were likely the same. A strong correlation was not observed between samples A and C and the two groups of black shale samples D and E, although both A and C showed high correlations with E, with A showing a moderate correlation. The rare earth partition curve showed that the curve trends of the

three samples are almost the same and show the same general trend. Therefore, the source and subsequent formation of the black shale and two kinds of ores are consistent. Bituminous sphalerite and the two groups of black shale from the Mayuan Zn-Pb mining area, especially the black shale from the Longmaxi Formation, are likely similar in terms of their sources and development processes over geological history. Furthermore, the migration of organic matter and metal elements during the mineralization processes of black shale and bituminous sphalerite were closely related. For example, research by Saintilan on the large MVT deposit in Lasvall, Sweden, showed that 40–60% of the Pb and Zn elements were derived from black shale, and a study on mineralization also showed that the key factor of activation and migration of Zn-Pb is the formation of hydrocarbon fluid by the thermal evolution of black shale [28]. The low pH of the acidic fluid is due to the Pb and Zn metal activation of a catalyst in black shale. Similarly, during the thermal evolution of the black shale before the “oil window” temperature is reached, organic matter is sourced from biological chemicals formed by the decomposition of organic acids (-COOH), and acidic and hydrocarbon fluid will result in the formation of a Pb and Zn organic complex and the accumulation of chloride from black shale in the basin structural trap [29,30]. Chloride then merges with hydrogen sulfide (H₂S) produced by the reaction between hydrocarbon fluids and sulfates, and precipitation occurs [31–33]. Previous studies have proposed that the key point of Zn-Pb mineralization is the migration of organic matter and metal elements. The correlation between the Mayuan Zn-Pb deposit and black shale indicates that the organic matter and metallogenic metal elements of the two ores were likely from the two groups of black shale, which provides an explanation for the high coincidence among the trends. Therefore, bitumen, asphaltic dolomite, and asphaltic sphalerite may have similar sources and development processes to the two groups of black shale in geological history. The Zn-Pb ores of Mayuan show a high content of metallic Zn elements, and are effectively carried by hydrocarbon fluids in the extraction experiment. The effective carrying of metal elements and hydrocarbon fluids sufficient to form MVT ore makes it reasonable for the two black shales to provide metal elements and organic matter for the Zn-Pb deposit of Mayuan. Therefore, in the actual ore-forming environment, the metal elements and some organic matter required by the lead-zinc ore of the Mayuan Zn-Pb deposit come from the two groups of black shale. After effectively carrying metal elements, it is then mixed with brine in a trap space for mineralization.

6. Conclusions

(1) It is found from the ICP data that the bitumen contains sufficient Zn elements to provide mineralization, and the data before and after the extraction experiment show that the hydrocarbon fluid effectively carries the metal elements in the sample. The organic matter in the Zn-Pb ore of Mayuan can be divided into two categories, among which the hydrocarbon organic matter is extracted in the extraction experiment. The remainder is combined with metallic elements in a non-hydrocarbon form to form metallic complexes.

(2) The results of the Pearson correlation coefficient show that the correlation between the Mayuan Zn-Pb deposit is very good. The rare earth partition curves of bitumen, asphaltic dolomite, and asphaltic sphalerite have the same trend and are very similar. It can be concluded that the formation environment and composition structure of the three ores are very similar, and it can be concluded that the asphaltic dolomite and asphaltic sphalerite all come from asphalt.

(3) The analysis found that black shale was a potential source rock; the Pearson correlation coefficient indicates that there is a strong correlation between the two black shale deposits, and that there is a moderate correlation between the Mayuan Zn-Pb deposit and the black shale. The rare earth fraction curves of the asphalt and the two black shales show the same trend and similar structure, indicating that the asphalt may come from the black shales of the Guojiaba Formation and the Longmaxi Formation. The two black shales may provide metal elements for the mineralization of the Mayuan Zn-Pb deposit.

Author Contributions: Conceptualization, S.L. and R.L.; methodology, S.L.; software, G.G.; validation, G.G. and S.L.; formal analysis, G.G. and S.L.; investigation, G.G. and S.L.; resources, R.L.; data curation, G.G.; writing—original draft preparation, G.G.; writing—review and editing, G.G. and S.L.; visualization, R.L.; supervision, R.L.; project administration, G.G. and S.L.; funding acquisition, S.L. and R.L. All authors have read and agreed to the published version of the manuscript.

Funding: This research work was supported by the National Natural Science Foundation of China (Nos. 41772118 and 42273064), The Innovative Research Team for Science and Technology of Shaanxi Province (2022TD-04), and the Natural Science Basic Research Program of Shaanxi Province (2022JQ-104).

Acknowledgments: We would like to thank the Key Laboratory of Western Mineral Resources and Geological Engineering of the Ministry of Education at Chang'an University for trace element analysis and testing by inductively coupled plasma analysis (ICP).

Conflicts of Interest: The authors declare no conflict of interest.

References

1. Dai, Z.X. The distribution types and exploration criteria of lead and zinc resources in the world. *World Nonferr. Metal.* **2005**, *3*, 15–23.
2. James, M.; Wood, H.S.; Omid, H.A.; Curtis, M.E.; Akai, T.; Currie, C. Solid bitumen in the Montney Formation; Diagnostic petro-graphic characteristics and significance for hydrocarbon migration. *Int. J. Coal Geol.* **2018**, *198*, 829–838.
3. Susan, R.; Keith, D.; Robert, S. Structural and diagenetic origin of breccias in the carbonate-hosted Polaris Zn-Pb deposit, Nunavut, Canada-Science Direct. *Ore Geol. Rev.* **2013**, *55*, 110–124.
4. Selby, D.; Creaser, R.A.; Dewing, K.; Fowler, M. Evaluation of bitumen as a IM Re-1MOs geochronometer for hydrocarbon maturation and migration: A test case from the Polaris MVT deposit, Canada. *Earth Planet. Sci. Lett.* **2005**, *235*, 1–15. [[CrossRef](#)]
5. Peter, N.L.; John, R.G. The effect of time changes in diagnosing lung cancer type on its recorded distribution, with particular reference to adenocarcinoma. *Regul. Toxicol. Pharm.* **2016**, *81*, 322–333.
6. Vandeginste, V.; Swennen, R.; Gleeson, S.A.; Ellam, R.M.; Osadetz, K.; Roure, F. Geochemical constraints on the origin of the Kicking Horse and Monarch Mississippi Valley-type lead-zinc ore deposits, southeast British Columbia, Canada. *Miner. Depos.* **2007**, *42*, 913–935. [[CrossRef](#)]
7. Chen, J.P.; Xiang, J.; Hu, Q.; Wei, Y.; Zili, L.; Bin, H.U.; Wei, W. Quantitative Geoscience and Geological Big Data Development. *Acta Geol. Sin.* **2016**, *90*, 1490–1515.
8. Gu, X.X.; Zhang, Y.M.; Li, B.H.; Xue, C.J.; Dong, S.Y.; Fu, S.H.; Cheng, W.B.; Liu, L.; Wu, C.Y. Coupling relationship between metal mineralization and hydrocarbon accumulation in sedimentary basins. *Earth Sci. Front.* **2010**, *17*, 83–105.
9. Gao, Y.B.; Li, K.; Qian, B.; WenYuan, L.; MinChang, Z.; Zhang, C. Trace elements, S, Pb, He, Ar and C isotopes of sphalerite in the Mayuan Zn-Pb deposits, at the northern margin of the Yangtze Plate, China. *Acta Petrol. Sin.* **2016**, *32*, 251–263.
10. Sverjensky, D.A. Genesis of Mississippi Valley Type lead-zinc deposits. *Annu. Rev. Earth Planet. Sci.* **1986**, *14*, 177–199. [[CrossRef](#)]
11. Huang, H.X.; Li, R.X.; Xiong, F.Y.; Hu, H.; Sun, W.; Jiang, Z.; Chen, L.; Wu, L. A method to probe the pore-throat structure of tight reservoirs based on low-field NMR: Insights from a cylindrical pore model. *Mar. Petrol. Geol.* **2020**, *117*, 104344. [[CrossRef](#)]
12. Huang, H.X.; Li, R.X.; Jiang, Z.X.; Chen, L. Investigation of variation in shale gas adsorption capacity with burial depth: Insights from the adsorption potential theory. *J. Nat. Gas. Sci. Eng.* **2020**, *73*, 103043. [[CrossRef](#)]
13. Miles, F.; Fiona, W.; Cathy, H. Fluid expulsion from over pressured basins: Implications for Pb, Zn mineralisation and dolomitisation of the East Midlands platform, northern England. *Mar. Petrol. Geol.* **2014**, *55*, 68–86.
14. Nicole, C.H.; Jacob, J.H.; Alexander, P.G. The role of hydrocarbons in ore formation at the Pillara Mississippi Valley type Zn-Pb deposit, Canning Basin, Western Australia. *Ore Geol. Rev.* **2018**, *102*, 875–893.
15. Chen, W.; Huang, Z.L.; Ye, L.; Hu, Y.; Santosh, M.; Wu, T.; He, L.; Zhang, J.; He, Z.; Xiang, Z.; et al. Genesis of carbonate-hosted Zn-Pb deposits in the Late Indosinian thrust and fold systems: An example of the newly discovered giant Zhugongtang deposit, South China. *J. Asian Earth Sci.* **2021**, *220*, 104–114.
16. Anderson, G. Kerogen as a source of sulfur in MVT deposits. *Econ. Geol.* **2015**, *110*, 837–840. [[CrossRef](#)]
17. Saintilan, N.J.; Spangenberg, J.E.; Chiaradia, M. Petroleum as source and carrier of metals in epigenetic sediment hosted mineralization. *Sci. Rep.* **2019**, *9*, 1–7. [[CrossRef](#)]
18. Yin, L. Mineralogical characteristics and genetic significance of Nanmushu Lead-zinc deposit in Mayuan area, Shaanxi Province, China. *Eng. Sci. Tech. Ser.* **2019**, *4*, 12–13.
19. Li, X.J.; Hou, M.T.; Zhu, Z.W. Prospecting model and prospect prediction of Guanyin lead-zinc deposit in the northern margin of Yangtze block. *Shaanxi Geol.* **2011**, *29*, 2–3.
20. Liu, S.W.; Liu, L.F.; Gao, Y.B.; Ge, X.H.; Zheng, X.Z.; Zhang, H.D.; Wang, L. Metallogenic material sources of the Mayuan lead-zinc deposit in the northern margin of Yangtze: Geochemical evidence from C, O, H, S, Pb and Sr isotopes. *Miner. Depos.* **2012**, *31*, 545–554.
21. Wang, X.H.; Xue, C.J.; Li, Z.M.; Li, Q.; Yang, R.J. Geological and geochemical characteristics of the Mayuan lead-zinc deposit in the northern margin of Yangtze landmass. *Miner. Depos.* **2008**, *27*, 37–48.

22. Li, H.M.; Chen, Y.C.; Wang, D.H. Li, H.Q. Geochemical characteristics and metallogenic age of Mayuan zinc deposit in Nanzheng area, Shaanxi Province. *Geol. Bull. China* **2007**, *26*, 546–552.
23. Li, R.X.; Dong, S.W.; Zhang, S.N.; Zhu, J.R.; Xia, B. Study on organic fluids during orogenic process in Daba Mountain. *J. Nanjing Uni.* **2012**, *48*, 295–307.
24. Li, R.X.; Qin, X.L.; Dong, S.W.; Shuwen, L. Characteristics of hydrocarbon fluid inclusions and significance for Evolution of Petroleum systems in the Dabashan Foreland, Central China. *Acta Geol. Sin.* **2015**, *89*, 861–875.
25. Boynton, W.V. Cosmochemistry of the Rare Earth Elements, In: Hcnderson P cd, Rare Earth Element Geochemistry. *Devel. Geochem.* **1984**, *2*, 3–114.
26. Manning, D.A.C.; Gize, A.P. The role of organic matter in ore transport processes. In *Organic Gechemistry: Principles and Application*; Engel, M.H., Macko, S.A., Eds.; Plenum Press: New York, NY, USA, 1993; pp. 547–563.
27. Li, D.L. Geochemical characteristics and paleosedimentary environment of Chang 7 oil shale in Triassic Yanchang Formation, southern Ordos Basin. *Basic Science. Eng. Sci. Tech. Ser.* **2019**, *12*, 53–58.
28. Saintilan, N.J.; Spangenberg, J.E.; Samankassou, E.; Kouzmanov, K.; Chiaradia, M.; Stephens, M.B.; Fontboté, L. A refined genetic model for the Laisvall and Vassbo MVT-type sandstone-hosted deposits, Sweden: Constraints from organic geochemistry. *Miner. Depos.* **2016**, *51*, 639–664. [[CrossRef](#)]
29. Eisenlohr, B.N.; Tompkins, L.A.; Cathles, L.M.; Groves, D.I. Mississippi Valley-type deposits: Products of brine expulsion by eustatically induced hydrocarbon generation. *Geology* **1994**, *22*, 315–318. [[CrossRef](#)]
30. Pelch, M.A.; Appold, M.S.; Emsbo, P.; Bodnar, R.J. Constraints from fluid inclusion compositions on the origin of Mississippi Valley-type mineralization in the Illinois-Kentucky district. *Econ. Geol.* **2015**, *110*, 787–808. [[CrossRef](#)]
31. David, A.B. Transport of metals by hydrocarbons in MVT deposits. *Acta Geol. Sin.* **2014**, *88*, 145–146.
32. Larbi, R.; Nejib, J.; Emmanuel, J.M.C. Organic matter and metal contents within the Cretaceous rocks of the Slataguern Halfaya area, North-Central Tunisia: Implication for ore genesis. *Ore Geol. Rev.* **2019**, *113*, 1–18.
33. Giordano, T.H. Transport of Pb and Zn by carboxylate complexes in basinal ore fluids and related petroleum- field brines at 100 °C: The influence of pH and oxygen fugacity. *Geochem. Trans.* **2002**, *3*, 56–72. [[CrossRef](#)] [[PubMed](#)]

Disclaimer/Publisher’s Note: The statements, opinions and data contained in all publications are solely those of the individual author(s) and contributor(s) and not of MDPI and/or the editor(s). MDPI and/or the editor(s) disclaim responsibility for any injury to people or property resulting from any ideas, methods, instructions or products referred to in the content.